Journal of
Composites Science

MDPI

Article

Cationic Polymerized Epoxy and Radiation Cured Acrylate Blend Nanocomposites Based on WS_2 Nanoparticles—Part A: Curing Processes and Kinetics

Gilad Gershoni [1], Hanna Dodiuk [1], Reshef Tenne [2] and Samuel Kenig [1,*]

[1] Department of Polymer Materials Engineering, Shenakr College, Ramat Gan 5252626, Israel
[2] Weizman Institute of Science, Rehovot 7610001, Israel
* Correspondence: samkenig@shenkar.ac.il

Abstract: Cationic photo-initiated and polymerized epoxies are characterized by good adhesion, high modulus, zero volatiles, low shrinkage and living polymerization characteristics. Radiation—cured acrylate resins are characterized by rapid initial curing with increased initial strength. The combination of radiation-cured acrylates and epoxies may present advantageous attributes. Thus, the system investigated is a hybrid epoxy/methyl acrylate and three different initiators for cationic polymerization of epoxies, the radical reaction of acrylates and the thermal initiator. When incorporating additives like opaque WS_2 nanoparticles (NPs), absorption of the photo radiation takes place, which may lead to low photo activity. Curing kinetics measurements revealed that the absorbing/masking effect of WS_2 was insignificant, and surprisingly, the level of curing was enhanced when the WS_2 NPs were incorporated. FTIR results demonstrated that covalent bonds were formed between the inorganic fullerenes (IF-WS_2) and the crosslinked matrix. Viscosity measurements showed a surprising reduction of five to ten times in the low-shear viscosity upon NPs incorporation compared to neat resins. It was concluded that the decrease of viscosity by the inorganic NPs, in addition to the enhanced level of conversion, has profound advantages for structural adhesives and 3D printing resins. To the best of our knowledge, this investigation is the first to report on a radiation-induced curing system containing opaque WS_2 NPs that leads to an enhanced degree of curing and reduced shear viscosity.

Keywords: cationic curing; radiation-induced; epoxy; acrylate; nanocomposite; tungsten disulfide nanoparticles

Citation: Gershoni, G.; Dodiuk, H.; Tenne, R.; Kenig, S. Cationic Polymerized Epoxy and Radiation Cured Acrylate Blend Nanocomposites Based on WS_2 Nanoparticles—Part A: Curing Processes and Kinetics. *J. Compos. Sci.* **2023**, *7*, 41. https://doi.org/10.3390/jcs7010041

Academic Editor: Tien-Thinh Le

Received: 21 October 2022
Revised: 16 December 2022
Accepted: 6 January 2023
Published: 16 January 2023

1. Introduction

Epoxy resins are well known and widely used in a wide range of industries such as aerospace, automotive, construction, microelectronics, defense, additive manufacturing, marine and more. Epoxy resin's popularity is attributed to its large variety of properties and enhanced adhesion to meet a wide range of end-product applications.

Cationic curing (CC) of epoxy gained attention in the past three decades. During this time, photoinitiator systems of the cationic polymerization reaction have been studied, offering advantages compared to the thermal curing of epoxies. The advantages include low energy consumption required for curing, rapid curing cycles, no need for solvents and curing upon demand. CC epoxy cures through a ring opening mechanism (ROP) [1–7] initiated by radical or cationic moieties [8,9] generated by the photolysis of photoinitiators (PIs). The photolysis-based products essentially generate a cationic moiety that initiates the ROP curing of the epoxy. Each PI has its intrinsic absorbance spectrum, which makes the CC process highly selective [8,10]. The selectivity of the PIs makes the CC resins ideal for applications requiring long pot life and curing on demand. The mechanism of the PIs was depicted in the 1970's [11,12]. The photolysis products generate a cationic moiety that initiates the ROP curing of the epoxy by charge transfer. The activated monomer reacts with

adjacent monomers to form a polymer network; hence propagation and chain-growth polymerization is initiated. For cationic curing to take place, the monomers must be nucleophilic and must form a stable cation during polymerization by protonation. PIs for cationic curing of epoxies were studied by Crivello during the 1970′s [11,12]. Photo acid generators (PAGs) are a key component for successful radiation cationic-cured epoxy. PAGs are composed of an anion moiety and a cation moiety. The cation moiety determines the photo-reactivity of the PIs and the efficiency of the radiation absorption. The anion moiety controls the strength of the photo acid, which influences the curing kinetics. The more stable and non-nucleophilic cation generated, the faster will be the curing reaction. Initially, Crivello used 3 PIs for cationic photocuring of epoxy: ArylDiazonium salt, TriarylSulfonium salt and DiphenylIodonium. ArylDiazonium salt is a strong Lewis acid, which generates N_2 as a byproduct and limits its use for thin coating only. TriarylSulfonium and DiphenylIodonium salts are strong Bronsted acids. Triaryl sulfonium salt and DiphenylIodonium salt are widely applied due to their high efficiency and stability during storage and upon heating. These initiators also exhibit high stability during storage in reactive epoxide monomers [13]. Triaryl sulfonium salt and DiphenylIodonium salt were also reported by Chen et al. [14]. Triaryl sulfonium salt and DiphenylIodonium salt absorb radiation at a wavelength range of 220–310 nm [8]. Known anionic moieties for PAGs (per-fluorinated compounds) are classified according to their reactivity [11]: BF_4^- < PF_6^- < AsF_6^- < SbF_6^-. Cationic curing process proceeds by different mechanisms. The mechanisms controlling the curing are set by the PI systems that are activated in a wide range of wavelengths. New PIs chemistries and their combinations were proposed over the years. Figure 1 summarizes the cationic mechanism, as described by Crivello for $Ar_3S^+X^-$ initiator [11]. Cationic polymerization starts by generating reactive species from the PIs. Specifically, upon direct photolysis of the PI (Step a), the onium salt dissociates into an anionic moiety (Step b) which evolves into a strong acid by abstracting hydrogen from adjacent monomer (Step c) and forming a cationic moiety. Onium salt dissociations are very efficient [8,9]. The anionic moiety stabilizes the positive charge generated on the epoxide ring. At this point, propagation starts with a nucleophilic attack of adjacent oxygen by the positively charged oxirane ring. The propagation step is efficient due to a combined effect of the positively charged oxirane ring and thermodynamically driven ring opening. The epoxy ring opening mechanism can theoretically keep on until no free monomers are left. This mechanism can be referred to as a living polymerization. Thus, polymerization may continue even in the absence of radiation after the initiation stage.

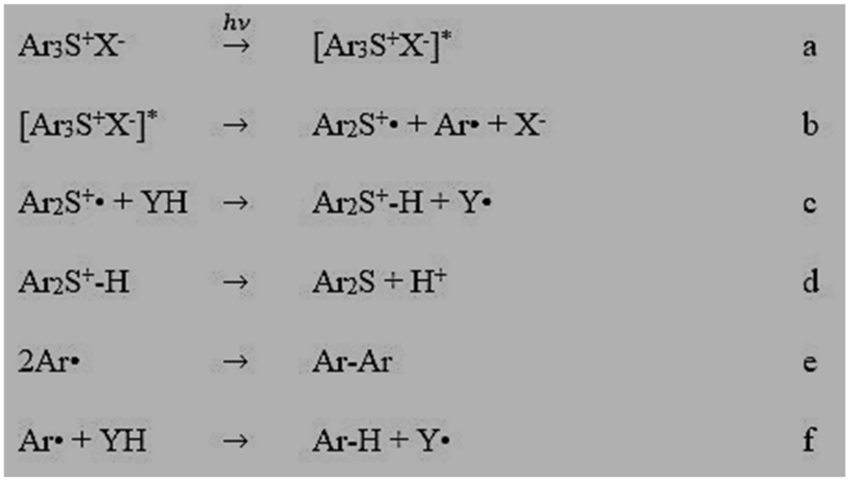

Figure 1. Cationic photocuring initiation mechanism. Reprinted (adapted) with permission from Crivello, J V (General Electric), "The Photoinitiated Cationic Polymerization of Epoxy Resins". Copyright (1979) American Chemical Society.

Where X is the anion moiety and YH is the monomer. At stage d, the release of proton H^+ takes place, thereby creating X^- the strong Bronsted acid required for cationic curing of the epoxy resin. Termination may be obtained as described by step e or continue to propagate as displayed by step f.

A summary of the initiator photolysis mechanism and the resulting epoxy curing process is described in Figure 2 through steps g, h, and i:

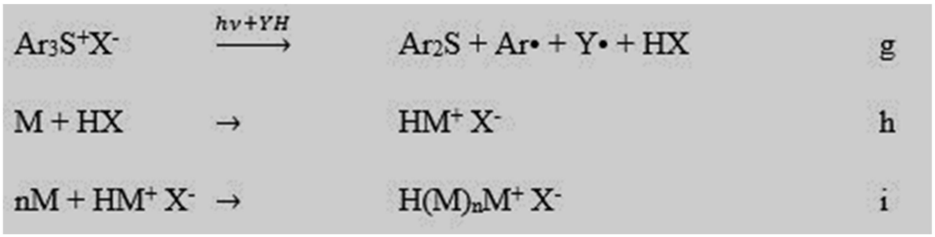

Figure 2. Cationic photocuring mechanism. Reprinted (adapted) with permission from Crivello, J V (General Electric), "The Photoinitiated Cationic Polymerization of Epoxy Resins". Copyright (1979) American Chemical Society.

Crivello suggested that the existence of acids in their anhydrous state is improbable. More likely, immediate protonation of the monomer [M] occurs to create $HM^+ X^-$ moiety, which is the start of the propagation stage. Others also reported on such curing mechanisms [14,15]. Due to the CC's inherent advantages, many studies were carried out to enrich the database of monomers and PIs used in the curing process [1,5,7,10,13,16–43]. The successful improvements of the CC process enabled its use in various industrial applications, such as in food packaging, adhesives, coatings, dental and 3D printing [14,19,44–50], and enlarged the resin selection [51]. The disadvantage of CC epoxy resins is their brittleness and low fracture toughness. Hence, a few studies were conducted aiming to improve the toughness of the CC epoxies [52]. Among a variety of methods, nanoparticles (NPs) were investigated as means to enhance the toughness of epoxies. It was shown that the dispersion quality of the NPs strongly affects the final CC resin properties [52–55]. The dispersion techniques used were high shear mixers, three roll mills [56,57], sonication and more. In several works, combinations of dispersion techniques were employed in order to achieve maximum dispersion quality. The modification of NPs surface chemistry may also affect the nanocomposite's final properties and length of shelf life, according to different reports [2,22,58–62]. Some reports showed improved compatibility of the NPs achieved through a surface modification that led to improved dispersion quality but led to inferior mechanical properties of the nanocomposites [58]. Improved toughness characteristics were reported in cases where the NPs were prepared insitu in the resins [2,3,21,63,64]. Since the IF-WS_2 NPs are opaque, the masking effect of this class of NPs could possibly introduce a major challenge. Thus, the dispersion techniques, dispersion quality and curing kinetics were major objectives of the present study.

2. Materials and Samples Preparation

2.1. Materials

Epoxy resin—(EPV 3420TX, supplied by Polymer Gvulot, Gvulot, Israel) was used and designated as PGE. EPV 3420TX without the thermal additive (Supplied by Polymer Gvulot, Israel) was designated as PGEnTA. The resins were composed of aliphatic epoxy (50 wt.%), methyl acrylate (10 wt.%), epoxy acrylate (15 wt.%), polyester polyol (15 wt.%) and fumed silica (5 wt.%). A special tri-photo-initiator blend (5 wt.%) was used consisting of sulfonium-based cationic PI, radical PI and thermal cationic initiator. The latter was removed for the PGEnTA resins. As can be seen, the resin is a hybrid epoxy/acrylate blend. The acrylate portion was designed for rapid initial curing. These resins were designed to cure in 395 nm wavelength irradiation of a light-emitting diode (LED).

Inorganic fullerenes, which are composed of hollow multi-layer nanoparticles– shortly designated as IF-WS_2 NPs from two suppliers were used: WS_2-TO (prepared at the Weizmann Institute of Science, Israel). These (quasi) spherical NPs were synthesized and used in another study [65]. The NPs have an average diameter of 80 nm and a hollow core with an interlayer spacing of 6.26 Å. A commercial powder of WS_2-C NPs with an irregular oval shape was purchased (M K Impex Corp, Missisauga, Canada). Sequential scanning electron microscopy (SEM) and powder X-ray diffraction (XRD) analyses revealed that these NPs had oval shapes with many irregularities (defects), and the interlayer spacing was 6.22 Å. The average particle size specified by the manufacturer is 90 nm (MKN-WS2-090).

The NPs were used as received and analyzed by a variety of methods, as summarized in Table 1.

Table 1. Intrinsic properties of the WS_2 NPs.

Comparison Criteria	WS_2-TO	WS_2-C
Geometry (*d*-space- interlayer layer spacing according to XRD)	Spherical (2θ = 14.1°; 6.26 Å)	Oval (2θ = 14.2°; 6.22 Å)
Diameter	80 nm	90 nm
Moisture Content	6.7% weight loss	1.5% weight loss
pH value	4.9	7.2
Oxygen/Tungsten ratio by XPS	0.55	0.83

2.2. Dispersion and Distribution Techniques

Two distinct procedures were utilized to study the dispersion and distribution of the WS_2 comprising Sonification/Vortex and masterbatch preparation. Results were evaluated by optical microscope (Coolpix MDC Lens by Nikon Japan, Tokyo, Japan). The optical microscope resolution can identify NPs of 0.8 μm in size.

2.3. Sonication/Vortex Multistage Dispersion Technique

The NPs were initially ground by mortar and pestle and then added to the resin in the desired quantity. A multistage combination was used employing a high-intensity horn-sonicator (Q700, Qsonica L.L.C, Newtown, CT, USA). Sonication resulted in a good dispersion. The distribution was accomplished by intensive Vortex mixing (Wizard IR Infrared Vortex Mixer, VELP Scientifica, Usmate, Italy) for a duration of 2 min at 3000 RPM. Ice-cooling was employed during this multistage dispersion procedure in order to keep the viscosity as high as possible under the high shearing rates used for the dispersion of the NPs. Ice-cooling was also exercised to prevent pre-curing of the resins during dispersion. Several repetitive stages were applied to enhance the dispersion quality.

2.4. Master-Batch Technique

In this method, 33,000 RPM was used by a grinding tool with an adequate vessel (Dremel 3000, Robert Bosch Tool Corporation, IL, USA). The attribute of the tool is its high shear mechanism. High-density compound (2:1 ratio of resin to NPs, respectively) was processed at 33,000 RPM for 20 min. This process was followed by 6 stages of Vortex/Horn-sonication for final dispersion. Samples were ice-cooled to avoid an increase in the temperature. The high-concentration master-batch method proved to be short 10 times compared to the multistage sonication/vortex method. Upscaling of the master-batch method could be easily achieved.

All prepared formulations were stored in a dark refrigerated environment to avoid a pre-curing reaction.

2.5. Curing System

The curing was done under 395 nm wavelength LED irradiation. Curing of all samples, excluding the sheared specimens, was done in a transparent silicone mold (SORTA-Clear 40,

Smooth-On, PA, USA) with specifically designed cavities covered by the same transparent silicone cover. A schematic illustration of the curing system can be found in Figure 3. The distance of the mold from the LED source was ~40 mm (near the side). A reflecting mirror was placed below the specimen and affected the curing of the bottom side of the sample (far side). The LED radiation intensity, according to the technical specification, is 7 W/cm^2.

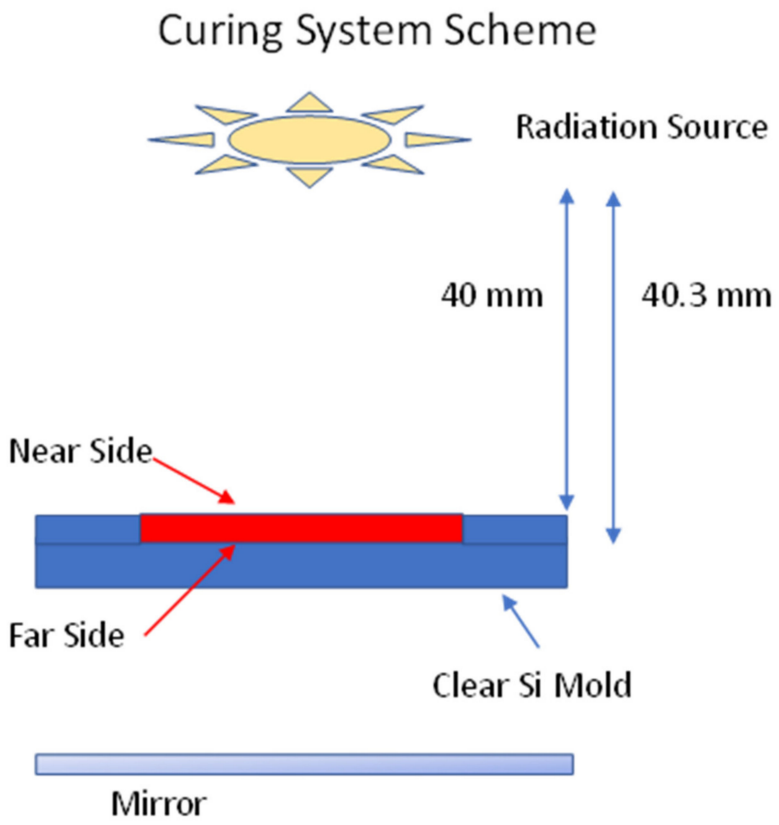

Figure 3. Schematic illustration of the curing system.

2.6. Kinetic Analysis of the Curing

The conversion level of the near side and the far side was followed by FTIR (Fourier transform infrared) spectra, and the difference between the near and the far sides were evaluated in order to analyze the masking effect. Attenuated Total Reflectance (ATR) FTIR (Bruker Alpha-T, Billerica, MA, USA) was employed to investigate the curing kinetics. Scanning ranged from wave number 375 to 4000 cm^{-1}. The spectrum was gathered by averaging over 40 scans at a resolution of 2 cm^{-1}.

The degree of conversion (DC) was calculated according to Equation (1).

$$DC = 100\ X\left(1 - \frac{normalized\ polymer\ oxirane\ ring}{normalized\ monomer\ oxirane\ ring}\right) \quad (1)$$

The data were normalized with respect to the unchanging alkyl group peak at 2820–2960 cm^{-1}. The oxirane peak is located at 770–830 cm^{-1}. The accuracy of the degree of conversion was determined as 0.5% to 1.0%.

The weight fractions of WS_2 were: 0, 0.3, 0.5, 0.75 and 1.0 wt.%. In order to study the curing kinetics, the duration of the radiation was varied as follows: 10, 20, 30, 60 and 120 s. Samples dimensions were 25 × 6 × 0.3–0.4 mm.

2.7. Thermal Curing Procedure

Thermal curing analysis was based on the differential scanning calorimetry (DSC) technique (~4 mg resin specimens). The DSC ramp was at 20 °C/min from 0 to 200 °C and

cooling at the same rate (DSC Q200, TA Instruments, New Castle, DE, USA). Following the DSC procedure, the cured resin was evaluated by FTIR to determine the DC.

2.8. IF-WS_2/Epoxy Interphase Analysis

In order to observe possible S-C and S=C covalent bonding, special specimens were prepared to contain 10 wt.% of IF-WS_2 NPs, which led to an enhanced FTIR signal. The samples were cured for 120 s.

2.9. Rheometry

The rheological properties of the various formulations at 25 °C were characterized using parallel plates with a diameter of 25 mm and a gap of 0.5 mm (Discovery HR-1, TA Instruments, New Castle, DE, USA). The frequency sweep was performed from 0.01 to 100 Hz.

2.10. Spectrophotometry

The absorbance spectrum measured at UV-Visible spectrum was done by a spectrophotometer from 440 to 360 nm (UV-1650PC, Shimadzu, Japan).

3. Results and Discussions

3.1. Pre-Cured Resin Properties

Preliminary characterization of the PGE and PGEnTA was performed by ATR-FTIR absorption and DSC measurements. Pre-cured resin showed similar UV- Visible spectra of the two resins (Figure 4 top). Following DSC thermal curing at a maximum of 250 °C, clear differences between the two resins can be observed in Figure 4 (bottom):

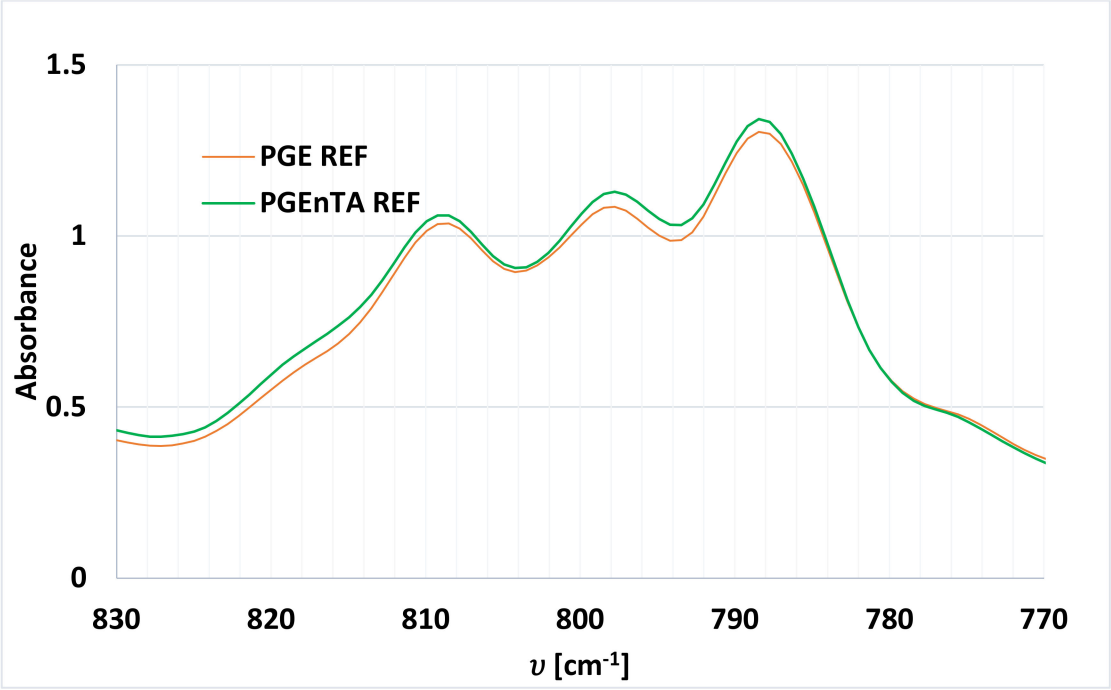

Figure 4. *Cont.*

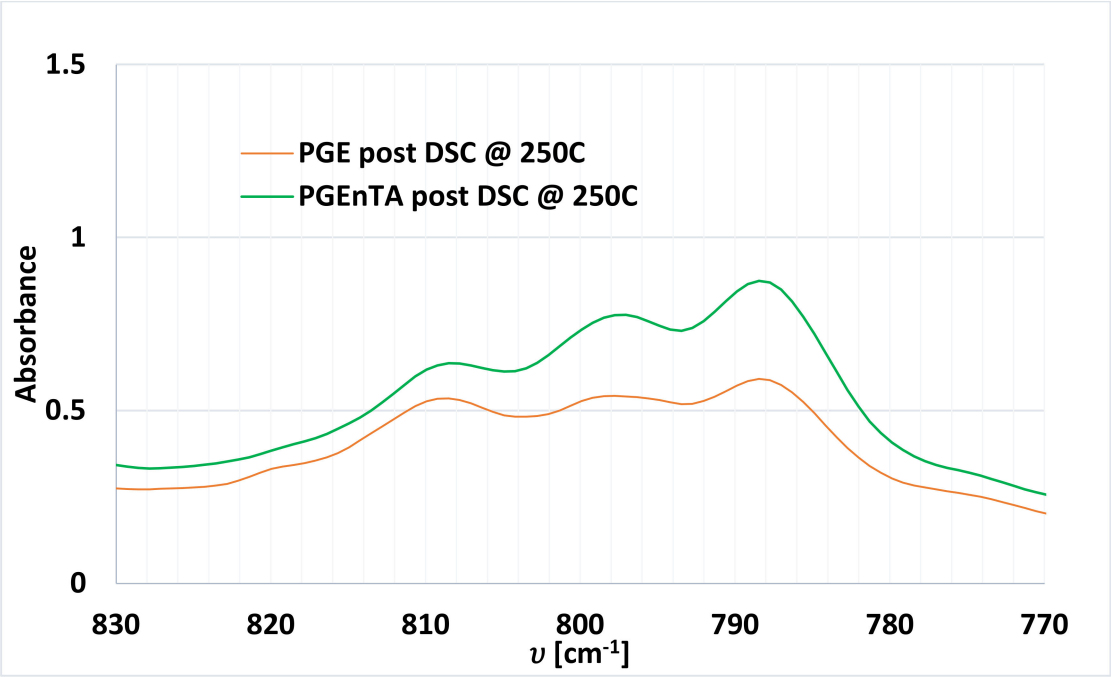

Figure 4. Pre-cured FTIR spectrum (**top**) and thermally post cured spectrum (**bottom**) of neat PGE and PGEnTA formulations.

It should be emphasized that the thermally induced DC obtained was 64% and 48% for PGE and PGEnTA, respectively. Although PGEnTA should not have displayed any thermal curing, it was found to be partially cured. Thermal curing of PGEnTA could occur by making the oxirane ring of the epoxy more liable for adjacent oxirane ring nucleophilic attack. Another possible reason for the curing is the creation of thermally induced radicals from the cleavage of the PIs, which in turn, initiated the curing of the acrylate and epoxy.

Analysis of the dispersion process showed that WS_2-C was harder to disperse compared to WS_2-TO in PGE. This may be due to a difference in the sensitivity towards humidity (water absorption) of the WS_2-TO compared to the WS_2-C. Furthermore, when vacuum dried (70 °C and −10 mm Hg), the WS_2-TO was harder to disperse, probably owing to the elimination of moisture from the WS_2 surface.

Viscosity measurements of the nanocomposite formulations are presented in Figures 5 and 6.

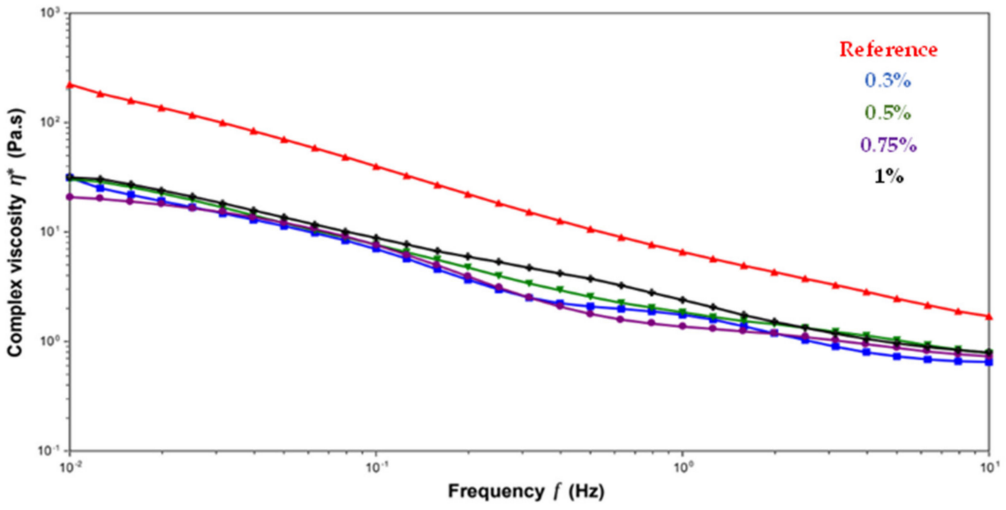

Figure 5. Complex viscosity of PGE with different loads of WS_2-TO at room temperature.

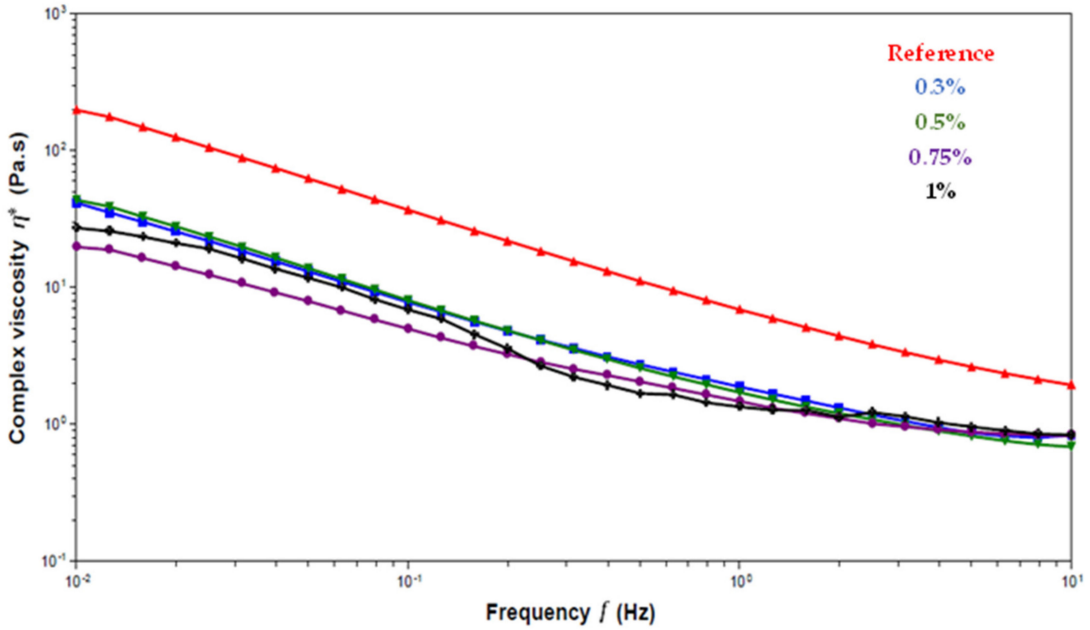

Figure 6. Complex viscosities of PGE with different loads of WS_2-C at room temperature.

Surprisingly, both WS_2 grades displayed a significant viscosity reduction, at low shear rates, from 200 Pa·s to 20–30 Pa·s. This viscosity reduction is unusual when compared to known data related to other NPs, which always demonstrate higher viscosity levels when incorporated into polymer resins. The reduced viscosity recorded for the epoxy blend containing the WS_2 NPs can be attributed to the lubrication effect of the WS_2 NPs, which induces facile shearing of the molecules on their surfaces.

3.2. Thermal Curing Kinetics

Thermal curing is affected by the thermal conductivity of IF-WS_2, which has not been reported yet in the literature. The thermal conductivity of single crystal WS_2 in the basal and out-of-plane was reported as 124 W/mK and 1.5 W/mK [66], respectively. The thermal conductivity of neat epoxy is ~0.15 W/mK [67]. Hence, the thermal conductivity of the resin is bound to improve. Therefore, IF-WS_2 was expected to enhance the thermal curing of the epoxy resin.

The DC of thermally cured composite and neat epoxy/acrylate formulations, using the DSC procedure, are depicted in Table 2.

Table 2. The degree of conversion (DC) and the exothermic peak temperature of thermally cured composite and neat epoxy/acrylate formulations.

Sample Name	PGE	PGEnTA Neat	PGEnTA 1.0 wt.% WS_2-C	PGEnTA 1.0 wt.%WS_2-TO
DC [%]	64	40	45	55
Exo. Peak [°C]	121	166	160	145

All PGE samples with WS_2-TO showed an exothermic peak at 134 °C, which started its elevation at 121–124 °C. The PGEnTA sample showed an increased risk of the exothermic peak at 166 °C, 160 °C and 145 °C for neat, 1.0% WS_2-C and 1.0 wt.% WS_2-TO, respectively. WS_2-TO shows the earliest and highest rise among the PGEnTA samples.

Prior to photocuring kinetics measurements, the absorbance of the various formulations was studied for a better understanding of the NPs effect on it. The absorbance results are presented in Figure 7.

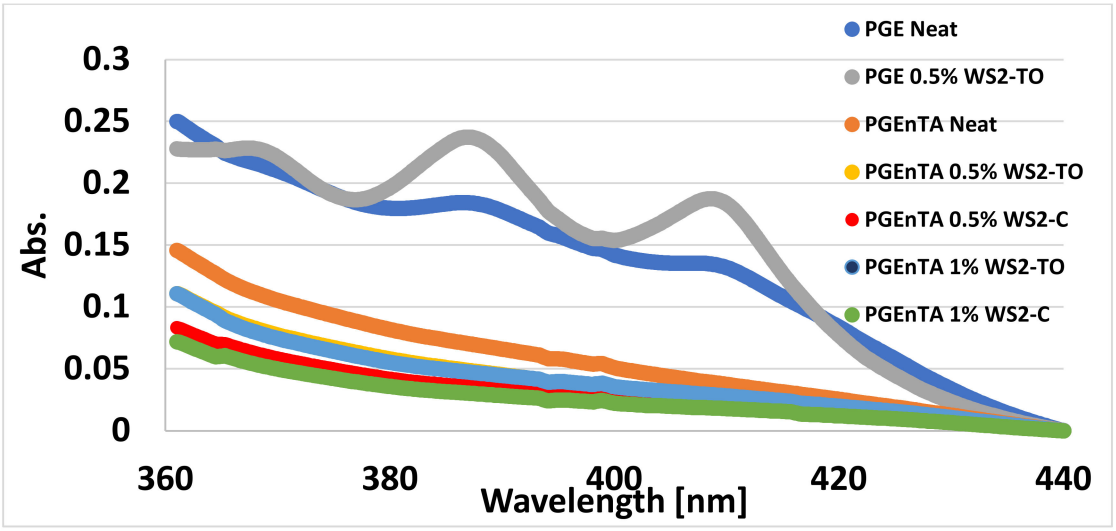

Figure 7. The absorption spectrum of selected cured epoxy/acrylate composite and neat formulations.

As can be observed in Figure 7, neat PGE shows the highest absorption than neat PGEnTA. It seems that the thermal additive (TA) affected the absorbance.

Furthermore, PGE with 0.5 wt.% WS_2-TO shows higher absorption, as is the case for 0.5 wt.% for the WS_2-C (not shown), which agrees with the masking effect by the NPs. In contrast, by incorporating of NPs into PGEnTA, the absorbance is decreased.

As can be noticed in Figure 8, for short curing times (up to 60 s), PGE exhibited higher DC on the rear side, and for longer curing times, PGEnTA reached the same level as the DC.

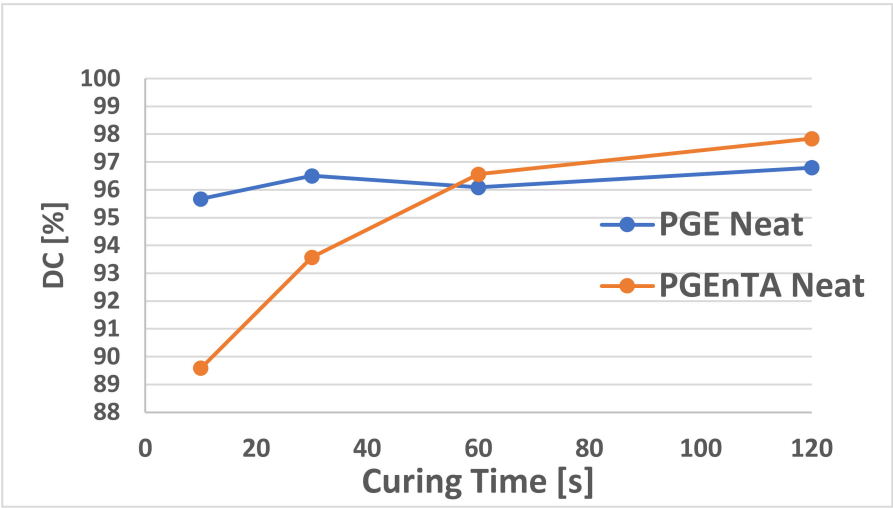

Figure 8. Curing kinetics of neat PGE and PGEnTA epoxy/acrylate formulations.

The relative constant value of the PGE DC compared to the gradual increase of the DC of the PGEnTA is attributed to its higher absorbance, which in turn affects the PIs photolysis efficiency. By this reasoning, TA enhances the curing, but as curing time proceeds beyond 30 s, the low absorption of the PGEnTA enables the radiation to penetrate deeper into the bulk of the resin, thereby increasing the DC on the far side. Absorption may lead to an enhanced masking effect or increase the PIs photolysis efficiency. Alternatively, diffusion of the reactive moieties deeper in the film allows a gradual increase in the penetration depth of the polymerization reaction.

NPs/Resin interphase analysis was done by preparation of 10 wt.% IF-WS_2 samples. The analysis was based on FTIR. Raichman et al. [68] indicated that the 1267 cm^{-1} peak

corresponds to the C=S bond and the 867 cm^{-1} peak to the C-S bond. Hence, the samples containing 10% of WS_2-C and WS_2-TO NPs in PGE and 10% WS_2-TO NPs in PGEnTA exhibited the 867 cm^{-1} peak, which was also obtained for the neat samples. This was attributed to PI/epoxy covalent bonding (the PI contains a sulphur atom). At 1267 cm^{-1} peak led to a different result compared to the 867 cm^{-1} peak, as can be observed in Figure 9.

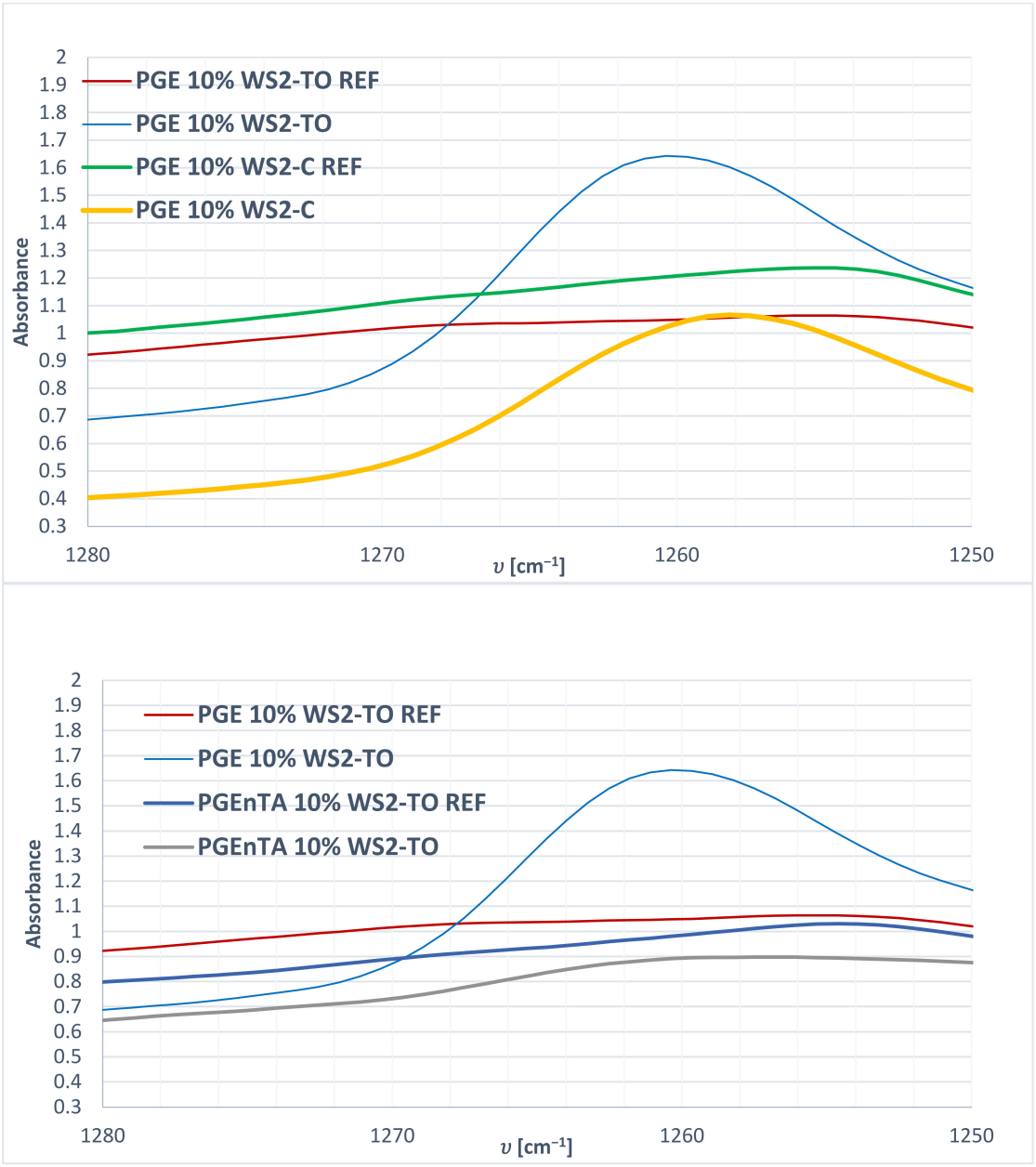

Figure 9. Expanded IR spectrum near the 1260 cm^{-1} peak for 10 wt.% of WS_2-TO and WS_2-C in PGE (**top**) and for 10 wt.% of WS_2-TO in PGE and PGEnTA. (**bottom**). REF refers to uncured resins.

It can be concluded that a clear C=S peak appears at ~1260 cm^{-1} for all types of cured IF-WS_2 NPs compared to the REF samples, which were uncured. Nonetheless, the intensity of the absorption peaks differed in their intensity from sample to sample. Hence, covalent bonding between the IF-WS_2 and the epoxy matrix was achieved.

Further analysis of the epoxy radiation-induced cationic curing indicated that high DC on the rear side and near side was obtained, reaching a value above 92% after 120 s curing, as can be seen in Figure 10.

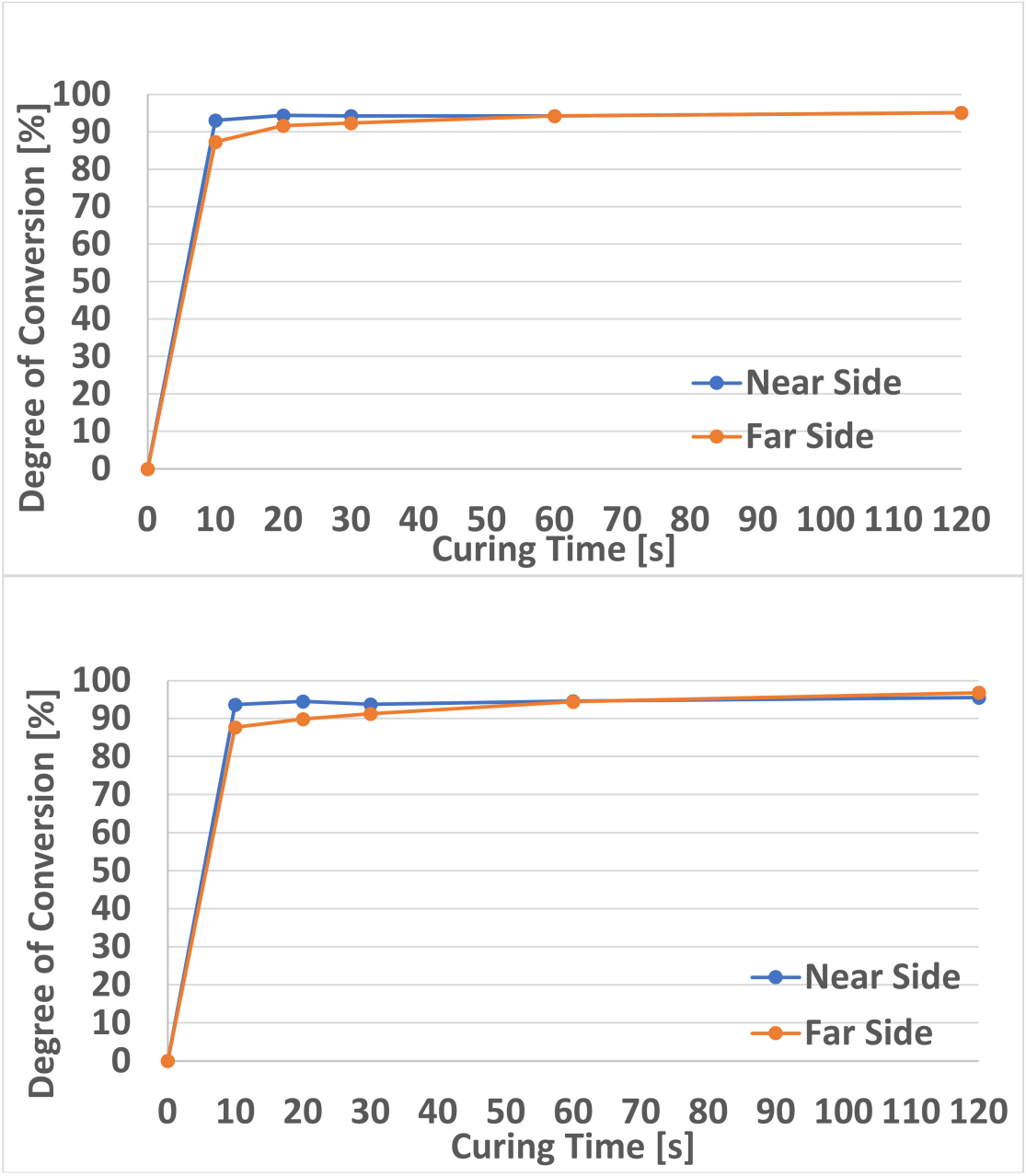

Figure 10. Curing kinetics of the photo-cured PGEnTA containing 0.75 wt.% of WS_2-C (**top**) and WS_2-TO (**bottom**) for near side and far side.

As can be observed, some masking effect is visible at short radiation times that disappears at sufficiently long curing times.

To study the masking effect, the difference between the DC of the near side and that of the rear side was determined. Hence, a positive differential means higher DC on the near side, indicating that masking did occur. A negative differential means higher DC on the rear side, indicating no masking effect. It can be observed in Figure 11 that a masking effect takes place for both resins when incorporating the WS_2-TO. NCs based on PGE exhibit a higher masking effect in lower NPs content, and PGEnTA-based NCs exhibit a higher masking effect in higher NPs content.

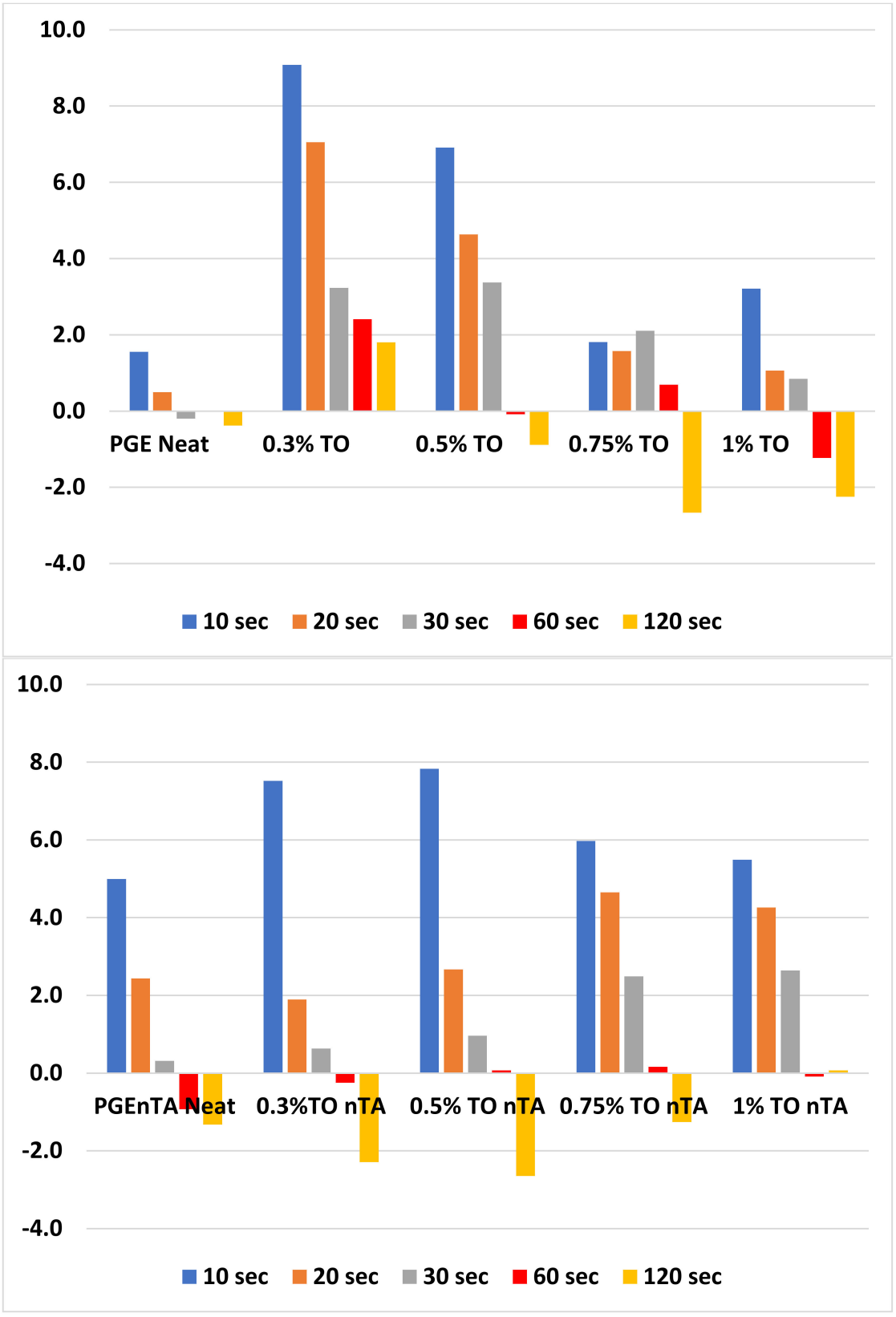

Figure 11. The differential DC between the near side and far side for PGE (**top**) and PGEnTA (**bottom**) with WS_2-TO at various concentrations.

Furthermore, as curing time increases, the masking effect is minimized for both resins. WS_2 is especially beneficial in eliminating the masking effect in PGE. This maybe due to the heating caused by the intense radiation that may trigger thermal curing.

In an additional stage of the study, the masking effect of WS_2-C dispersed in PGEnTA was carried out. As evident in Figure 12 and in contrast with WS_2 –TO results, the WS_2 –C NPs addition resulted in a masking effect even after long curing times. This may be due to the oval shape of the WS_2-C NPs compared to the spherical shape of the WS_2-TO NPs. As can be observed from Figure 11, a high level of loading of WS_2–C (1.0 wt.%) with a long curing time (120 s) enables the DC level to match that of the neat sample.

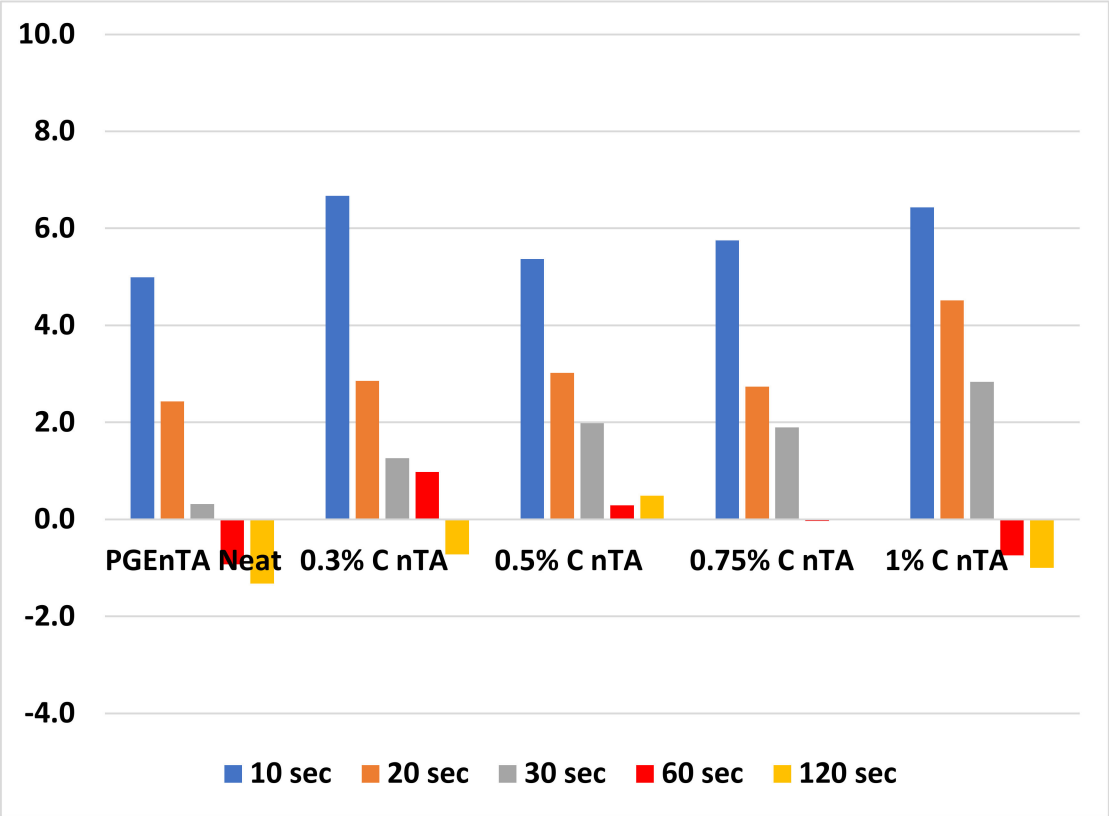

Figure 12. The DC differentials between the near side and far side of PGEnTA with WS_2-C at various concentrations.

As can be concluded, the photo-induced curing kinetics of RCNC is a complex process. The type of the WS_2 NPs affects the thermal and photo-induced curing kinetics as well as the resin formula.

4. Conclusions

WS_2 NPs have been shown to be beneficial for the cationic polymerized epoxy and radiation-curing acrylates blends. This unique inorganic fullerene exhibited two outstanding attributes. First, it caused a ten-fold decrease in the shear viscosity of the nanocomposite resins, and second, it exhibited enhanced curing kinetics. At high WS_2 levels (1% wt.), a masking effect was observed. However, at low WS_2 content, the DC was enhanced. Furthermore, the inorganic NPs formed covalent bonding with the epoxy resin. The two different sources of WS_2 NPs affected to a certain extent differently the curing kinetics. This difference can be ascribed to their geometrical differences, i.e., the spherical form of the WS_2 –TO vs. irregular oval morphology of the WS_2-C. To the best of our knowledge, this is the first study of radiation-induced curing containing opaque WS_2 NPs that leads to an enhanced degree of curing. The effect of the nanocomposite formulations and the curing

kinetics on the mechanical and thermal properties of the RCNC is of importance and will be reported in a separate publication.

Author Contributions: Conceptualization: H.D., S.K. and R.T.; Investigation: G.G. and H.D.; Writing: G.G.; Supervision: H.D., S.K. and R.T. All authors have read and agreed to the published version of the manuscript.

Funding: Innovation Authority of Israel and the Fraunhofer (Germany) research program, Grant No. 64772.

Acknowledgments: RT acknowledges the support of The Estate of Manfred Hecht and the Estate of Diane Recanati. He is also grateful to the Perlman Family Foundation, the Kimmel Center for Nanoscale Science.

Conflicts of Interest: The authors declare no conflict of interest.

References

1. Crivello, J.V.; Kong, S.; Jang, M. Cationic polymerization: New developments and applications. *Macromol. Symp.* **2004**, *217*, 47–61. [CrossRef]
2. Sangermano, M.; Voit, B.; Sordo, F.; Eichhorn, K.J.; Rizza, G. High refractive index transparent coatings obtained via UV/thermal dual-cure process. *Polymer* **2008**, *49*, 2018–2022. [CrossRef]
3. Sangermano, M.; Malucelli, G.; Amerio, E.; Bongiovanni, R.; Priola, A.; Gianni, A.D.; Voit, B.; Rizza, G. Preparation and characterization of nanostructured TiO_2/epoxy polymeric films. *Macromol. Mater. Eng.* **2006**, *291*, 517–523. [CrossRef]
4. Dabestani, R.; Ivanov, I.N.; Sands, J.M. *Cationic Polymerization (Cure Kinetics) of Model Epoxide Systems*; Army Research Laboratory: Adelphi, MD, USA, 2002.
5. Atif, M.; Bongiovanni, R.; Yang, J. Cationically UV-Cured Epoxy Composites. *Polym. Rev.* **2015**, *55*, 37–41. [CrossRef]
6. Crivello, J.V. UV and electron beam-induced cationic polymerization. *Nucl. Inst. Methods Phys. Res. B* **1999**, *151*, 8–21. [CrossRef]
7. Liu, G.; Zhu, X.; Xu, B.; Qian, X.; Song, G.; Nie, J. Cationic photopolymerization of bisphenol A diglycidyl ether epoxy under 385 nm. *J. Appl. Polym. Sci.* **2013**, *130*, 3698–3703. [CrossRef]
8. Crivello, J.V.; Sangermano, M. Visible and Long-Wavelength Photoinitiated Cationic Polymerization. *J. Polym. Sci. Part A Polym. Chem.* **2001**, *39*, 343–356. [CrossRef]
9. Crivello, J.V. Synergistic Free Radical Effects in Photoinitiated Cationic Polymerization. *Photoinitiated Polym.* **2003**, *847*, 178–186.
10. Aydogan, B.; Gacal, B.; Yildirim, A.; Yonet, N.; Yuksel, Y. Wavelength tunability in photoinitiated cationic polymerization. In *Photochemistry and UV Curing New Trends*; Fouassier, J.P., Ed.; Research Signpost: Trivandrum, Indian, 2006; Volume 661, pp. 1–15. ISBN 81-308-0014-4.
11. Crivello, J.V.; Lam, J.H.W. The Photoinitiated Cationic Polymerization of Epoxy Resins. *Am. Chem. Soc. Symp. Ser.* **1979**, *114*, 1–16. [CrossRef]
12. Crivello, J.V.; Lam, J.H.W. Diaryliodonium Salts. A New Class of Photoinitiators for Cationic Polymerization. *Macromolecules* **1977**, *10*, 1307–1315. [CrossRef]
13. Klikovits, N.; Knaack, P.; Bomze, D.; Krossing, I.; Liska, R. Novel photoacid generators for cationic photopolymerization. *Polym. Chem.* **2017**, *8*, 4414–4421. [CrossRef]
14. Chunfu, C.; Li, B.; Wang, C.; Iwasaki, S.; Kanari, M.; Lu, D. UV and Thermal Cure Epoxy Adhesives. In *Paint and Coating Indisutry*; Yilmaz, F., Ed.; Intech Open: London, UK, 2018; pp. 71–85.
15. Malik, M.S.; Schlogl, S.; Wolfahrt, M.; Sangermano, M. Review on UV-Induced Cationic Frontal Polymerization of Epoxy Monomers. *Polymers* **2020**, *12*, 2146. [CrossRef]
16. Schroeder, W.F.; Asmussen, S.V.; Sangermano, M.; Vallo, C.I. Visible light polymerization of epoxy monomers using an iodonium salt with camphorquinone/ethyl-4-dimethyl aminobenzoate. *Polym. Int.* **2013**, *62*, 1368–1376. [CrossRef]
17. Golaz, B.; Michaud, V.; Månson, J.A.E. Photo-polymerized epoxy primer for adhesion improvement at thermoplastics/metallic wires interfaces. *Compos. Part A Appl. Sci. Manuf.* **2013**, *48*, 171–180. [CrossRef]
18. Ryu, C.Y.; Spencer, M.J.; Crivello, J.V. Involvement of supramolecular complexes in the capture and release of protonic acids during the cationic ring-opening polymerization of epoxides. *Macromolecules* **2012**, *45*, 2233–2241. [CrossRef]
19. Vitale, A.; Sangermano, M.; Bongiovanni, R.; Burtscher, P.; Moszner, N. Visible light curable restorative composites for dental applications based on epoxy monomer. *Materials* **2014**, *7*, 554–562. [CrossRef]
20. Crivello, J.V.; Liu, S. Photoinitiated cationic polymerization of epoxy alcohol monomers. *J. Polym. Sci. Part A Polym. Chem.* **2000**, *38*, 389–401. [CrossRef]
21. Foix, D.; Ramis, X.; Sangermano, M.; Serra, A. Synthesis of a New Hyperbranched-Linear-Hyperbranched Triblock Copolymer and Its Use as a Chemical Modifier for the Cationic Photo and Thermal Curing of Epoxy Resins. *J. Polymer Sci. A Polymer Chem.* **2012**, *50*, 1133–1142. [CrossRef]

22. Belon, C.; Chemtob, A.; Croutxé-Barghorn, C.; Rigolet, S.; Schmitt, M.; Bistac, S.; Le Houérou, V.; Gauthier, C. Nanocomposite coatings via simultaneous organic-inorganic photo-induced polymerization: Synthesis, structural investigation and mechanical characterization. *Polym. Int.* **2010**, *59*, 1175–1186. [CrossRef]
23. Lalevée, J.; Mokbel, H.; Fouassier, J.P. Recent developments of versatile photoinitiating systems for cationic ring opening polymerization operating at any wavelengths and under low light intensity sources. *Molecules* **2015**, *20*, 7201–7221. [CrossRef]
24. Park, S.; Kilgallon, L.J.; Yang, Z.; Ryu, D.Y.; Ryu, C.Y. Molecular Origin of the Induction Period in Photoinitiated Cationic Polymerization of Epoxies and Oxetanes. *Macromolecules* **2019**, *52*, 1158–1165. [CrossRef]
25. Lecompère, M.; Allonas, X.; Maréchal, D.; Criqui, A. Dual-cure Photo-thermal Initiating System for Cationic Polymerization of Epoxy under LED Visible Light. *Photopolym. Sci. Technol.* **2017**, *30*, 399–404. [CrossRef]
26. Lecompère, M.; Allonas, X.; Maréchal, D.; Criqui, A. Versatility of Pyrylium Salt/Vinyl Ether Initiating System for Epoxide Dual-Cure Polymerization: Kick-Starting Effect of the Coinitiator. *Macromol. Rapid Commun.* **2017**, *38*, 1600660. [CrossRef] [PubMed]
27. Bomze, D.; Knaack, P.; Liska, R. Successful radical induced cationic frontal polymerization of epoxy-based monomers by C-C labile compounds. *R. Soc. Chem.* **2015**, *6*, 8161–8167. [CrossRef]
28. Mariani, A.; Bidali, S.; Fiori, S.; Sangermano, M.; Malucelli, G.; Bongiovanni, R.; Priola, A. UV-ignited frontal polymerization of an epoxy resin. *J. Polym. Sci. Part A Polym. Chem.* **2004**, *42*, 2066–2072. [CrossRef]
29. Park, H.J.; Ryu, C.Y.; Crivello, J.V. Photoinitiated cationic polymerization of limonene 1,2-oxide and α-pinene oxide. *J. Polym. Sci. Part A Polym. Chem.* **2013**, *51*, 109–117. [CrossRef]
30. Durmaz, Y.Y.; Moszner, N.; Yagci, Y. Visible light initiated free radical promoted cationic polymerization using acylgermane based photoinitiator in the presence of onium salts. *Macromolecules* **2008**, *41*, 6714–6718. [CrossRef]
31. Xiao, P.; Zhang, J.; Dumur, F.; Tehfe, A.M.; Morlet-Savary, F.; Graff, B.; Gigmes, D.; Fouassier, J.P.; Lalevée, J. Visible light sensitive photoinitiating systems: Recent progress in cationic and radical photopolymerization reactions under soft conditions. *Prog. Polym. Sci.* **2015**, *41*, 32–66. [CrossRef]
32. Zhang, J.; Campolo, D.; Dumur, F.; Xiao, P.; Fouassier, J.P.; Gigmes, D.; Lalevée, J. Visible-Light-Sensitive Photoredox Catalysis by Iron Complexes: Applications in Cationic and Radical Polymerization Reactions. *J. Polym. Sci. A Polym. Chem.* **2016**, *54*, 2247–2253. [CrossRef]
33. Zhang, J.; Dumur, F.; Horcajada, P.; Livage, C.; Xiao, P.; Fouassier, J.P.; Gigmes, D.; Lalevée, J. Iron-Based Metal-Organic Frameworks (MOF) as Photocatalysts for Radical and Cationic Polymerizations under Near UV and Visible LEDs (385–405 nm). *Macromol. Chem. Phys.* **2016**, *217*, 2534–2540. [CrossRef]
34. Lim, K.S.; Schon, B.S.; Mekhileri, N.V.; Brown, G.C.J.; Chia, C.M.; Prabakar, S.; Hooper, G.J.; Woodfield, T.B.F. New Visible-Light Photoinitiating System for Improved Print Fidelity in Gelatin-Based Bioinks. *ACS Biomater. Sci. Eng.* **2016**, *2*, 1752–1762. [CrossRef]
35. Wang, D.; Szillat, F.; Fouassier, J.P.; Lalevée, J. Remarkable Versatility of Silane/Iodonium Salt as Redox Free Radical, Cationic, and Photopolymerization Initiators. *Macromolecules* **2019**, *52*, 5638–5645. [CrossRef]
36. Haifaa, M.; Dumur, F.; Telitel, S.; Vidal, L.; Xiao, P.; Versace, D.L.; Tehfe, M.A.; Morlet-Savary, F.; Graff, B.; Fouassier, J.P.; et al. PhotoInitiating Systems of Polymerization and In-Situ Incorporation of Metal Nanoparticles in Polymer Matrixes Upon Visible Lights: Push-Pull Malonate and Malonitrile Based Dyes. *Polym. Chem.* **2013**, *4*, 5679–5687.
37. Hoppe, C.C.; Ficek, B.A.; Eom, H.S.; Scranton, A.B. Cationic photopolymerization of epoxides containing carbon black nanoparticles. *Polymer* **2010**, *51*, 6151–6160. [CrossRef]
38. Dickey, M.D.; Gupta, S.; Leach, K.A.; Collister, E.; Willson, C.G.; Russell, T.P. Novel 3-D structures in polymer films by coupling external and internal fields. *Langmuir* **2006**, *22*, 4315–4318. [CrossRef]
39. Sangermano, M.; Roppolo, I.; Chiappone, A. New horizons in cationic photopolymerization. *Polymers* **2018**, *10*, 136. [CrossRef]
40. Yagci, Y. Initiation of Cationic Polymerization by Photoinduced Electron Transfer. *Macromol. Symp.* **1998**, *134*, 177–188. [CrossRef]
41. Crivello, J.V.; Lee, J.L. Photosensitized Cationic Polymerizations Using Dialkylphenacylsulfonium and Dialkyl(4-hydroxyphenyl) sulfonium Salt Photoinitiators. *Macromolecules* **1981**, *14*, 1141–1147. [CrossRef]
42. Nelson, E.W.; Carter, T.P.; Scranton, A.B. The role of the triplet state in the photosensitization of cationic polymerizations by anthracene. *J. Polym. Sci. Part A Polym. Chem.* **1995**, *33*, 247–256. [CrossRef]
43. Crivello, J.V.; Ortiz, R.A. Benzyl alcohols as accelerators in the photoinitiated cationic polymerization of epoxide monomers. *J. Polym. Sci. Part A Polym. Chem.* **2002**, *40*, 2298–2309. [CrossRef]
44. Nakajima, A.; Tomotake, A.; Kida, S.; Konica Minolta IJ Technologies. Development of New Cationic UV Curable Inkjet Ink. 2006. Available online: https://www.konicaminolta.com/inkjet/technology/report/pdf/200809_ppic08.pdf (accessed on 20 October 2022).
45. Baikerikar, K.K.; Scranton, A.B. Photopolymerizable liquid encapsulants for microelectronic devices: Thermal and mechanical properties of systems with reduced in-mold cure times. *J. Appl. Polym. Sci.* **2001**, *81*, 3449–3461. [CrossRef]
46. Ligon, S.C.; Liska, R.; Stampfl, J.; Gurr, M.; Mülhaupt, R. Polymers for 3D Printing and Customized Additive Manufacturing. *Chem. Rev.* **2017**, *117*, 10212–10290. [CrossRef] [PubMed]
47. Eftekhari, A. Tungsten dichalcogenides (WS_2, WSe_2, and WTe_2): Materials chemistry and applications. *J. Mater. Chem. A* **2017**, *5*, 18299–18325. [CrossRef]

48. Sharif, M.; Pourabbas, B.; Sangermano, M.; Moghadam, F.S.; Mohammadi, M.; Roppolo, I.; Fazli, A. The effect of graphene oxide on UV curing kinetics and properties of SU8 nanocomposites. *Polym. Int.* **2017**, *66*, 405–417. [CrossRef]
49. Kim, Y.K.; Kim, S.K.; Kim, K.H.; Kwon, T.Y. Degree of conversion of dual-cured resin cement light-cured through three fibre posts within human root canals: An ex vivo study. *Int. Endod. J.* **2009**, *42*, 667–674. [CrossRef]
50. Pandey, R. Photopolymers in 3D Printing Applications. 2014. Available online: https://www.theseus.fi/bitstream/handle/10024/80083/pandey_ramji.pdf?sequence=1&isAllowed=y (accessed on 20 October 2022).
51. Verschueren, K.; Kaurb, B. Cycloaliphatic Epoxide Resins for Cationic UV-Cure. 1996. Available online: https://www.osti.gov/etdeweb/servlets/purl/20051955 (accessed on 20 October 2022).
52. Otorgust, G.; Sedova, A.; Dodiuk, H.; Kenig, S.; Tenne, R. Carbon and tungsten disulfide nanotubes and fullerene-like nanostructures in thermoset adhesives: A critical review. *Rev. Adhes. Adhes.* **2015**, *3*, 311–363. [CrossRef]
53. Haba, D.; Brunner, A.J.; Pinter, G. Dispersion of fullerene-like WS_2 nanoparticles within epoxy and the resulting fracture mechanics. *Compos. Sci. Technol.* **2015**, *119*, 55–61. [CrossRef]
54. Shneider, M.; Dodiuk, H.; Kenig, S.; Tenne, R. The effect of tungsten sulfide fullerene-like nanoparticles on the toughness of epoxy adhesives. *J. Adhes. Sci. Technol.* **2010**, *24*, 1083–1095. [CrossRef]
55. Haba, D.; Barbezat, M.; Ayalur-Karunakaran, S.; Schlögl, S.; Brunner, A.J.; Pinter, G. Significance of epoxy network properties for the toughening effect of flaky and fullerene-like WS_2 nanoparticles. *J. Polym. Sci. Part B Polym. Phys.* **2016**, *54*, 1738–1747. [CrossRef]
56. Haba, D. Toughening of Epoxy with WS_2 Nanoparticles. Ph.D. Thesis, Montanunitversitaet Leoben, Leoben, Austria, 2016. Available online: https://pure.unileoben.ac.at/portal/files/1835750/AC13362385n01vt.pdf (accessed on 20 October 2022).
57. Thostenson, E.T.; Chou, T.W. Processing-structure-multi-functional property relationship in carbon nanotube/epoxy composites. *Carbon N. Y.* **2006**, *44*, 3022–3029. [CrossRef]
58. Shneider, M.; Dodiuk, H.; Tenne, R.; Kenig, S. Nanoinduced Morphology and Enhanced Properties of Epoxy Containing Tungsten Disulfide Nanoparticles. *Polym. Eng. Sci.* **2013**, *53*, 2624–2632. [CrossRef]
59. Haba, D.; Griesser, T.; Müller, U.; Brunner, A.J. Comparative investigation of different silane surface functionalizations of fullerene-like WS_2. *J. Mater. Sci.* **2015**, *50*, 5125–5135.
60. Sangermano, M.; Priola, A.; Kortaberria, G.; Jimeno, A.; Garcia, I.; Mondragon, I.; Rizza, G. Photopolymerization of epoxy coatings containing iron-oxide nanoparticles. *Macromol. Mater. Eng.* **2007**, *292*, 956–961. [CrossRef]
61. Bongiovanni, R.; Turcato, E.A.; di Gianni, A.; Ronchetti, S. Epoxy coatings containing clays and organoclays: Effect of the filler and its water content on the UV-curing process. *Prog. Org. Coat.* **2008**, *62*, 336–343. [CrossRef]
62. Martin-Gallego, M.; Verdejo, R.; Lopez-Manchado, M.A.; Sangermano, M. Epoxy-Graphene UV-cured nanocomposites. *Polymer* **2011**, *52*, 4664–4669. [CrossRef]
63. Chemtob, A.; Versace, D.L.; Belon, C.; Croutxé-Barghorn, C.; Rigolet, S. Concomitant organic-inorganic UV-curing catalyzed by photoacids. *Macromolecules* **2008**, *41*, 7390–7398. [CrossRef]
64. Däbritz, F.; Voit, B.; Naguib, M.; Sangermano, M. Hyperstar poly (ester-methacrylate) s as additives in thermally and photocured epoxy resins. *Polymer* **2011**, *52*, 5723–5731. [CrossRef]
65. Tenne, R.; Margulis, L.; Genut, M.; Hodes, G. Polyhedral and cylindrical structures of tungsten disulphide. *Nature* **1992**, *360*, 444–446. [CrossRef]
66. Pisoni, A.; Jacimovic, J.; Gaál, R.; Náfrádi, B.; Berger, H.; Révay, Z.; Forró, L. Anisotropic transport properties of tungsten disulfide. *Scr. Mater.* **2016**, *114*, 48–50. [CrossRef]
67. Garrett, K.W.; Rosenberg, H.M. The thermal conductivity of epoxy-resin/powder composite materials. *J. Phys. D Appl. Phys.* **1974**, *7*, 1247–1258. [CrossRef]
68. Raichman, D.; Strawser, D.A.; Lellouche, J.P. Covalent functionalization/polycarboxylation of tungsten disulfide inorganic nanotubes (INTs-WS_2). *Nano Res.* **2015**, *8*, 1454–1463. [CrossRef]